Fusing Leontovich Boundary Conditions and Scalar 2D FEM to Compute Lid and Lateral Wall Losses in *H*-plane Waveguide Devices

Hui Jiang, Juan Córcoles, and Jorge A. Ruiz-Cruz

***Abstract*—This paper introduces a 2D finite element method (FEM) for *H*-plane waveguide devices, initially formulated for the ideal lossless case and then extended to include conductor losses. A scalar formulation naturally incorporates the Leontovich boundary condition on both the lid and lateral walls, with a first-order wavenumber correction at the lid walls and an additional matrix for lateral wall losses. Numerical results including an inductive filter and a K-band diplexer show excellent agreement with both analytic (when possible) and commercial software simulations based on 3D-FEM, confirming the method's accuracy and efficiency for practical waveguide device analysis and design.**

***Index Terms*—finite element method, *H*-plane waveguide devices, Leontovich boundary condition**

I. Introduction

Waveguide devices are fundamental components in many microwave and millimeter-wave systems, including couplers, filters and multiplexers. Accurate and efficient modeling of such devices is essential for the design and optimization of components for radar and communication systems [1]–[3].

On the one hand, traditional 3D full-wave electromagnetic solvers provide highly accurate solutions but often come with significant computational costs, especially for complex geometries, since they offer the highest flexibility in handling various boundary conditions and material properties. On the other hand, for simpler structures, simplified 2D methods, such as the 2D finite element method (FEM) [4], [5], have been widely explored to alleviate the computational burden without losing accuracy. In this context, the assessment of the conductor losses in the so-called *H*-plane waveguide devices (as the one represented in Fig. 1) has been traditionally carried out at the end of the design cycle, leaving their computations to 3D full-wave solvers. While the use of 2D FEM in the analysis of *H*-plane waveguide devices has been long known [6]–[8], and 2.5D methods have attracted recent attention [9], [10], specific formulations to take conductor losses into account with a scalar approach have not so far been proposed, to the best of the authors' knowledge, in a comprehensive manner.

Received 27 February 2025; This work was supported by Grant TED2021-130650B-C21 (ANT4CLIM) and Grant PID2023-146246OB-C31 (ANT4IT) funded in part by MICIU/AEI/10.13039/501100011033 (Agencia Estatal de Investigación), in part by UE (European Union) "NextGenerationEU"/PRTR, and in part by FEDER/UE.

Hui Jiang is with Departamento de Tecnología Electrónica y de las Comunicaciones, Escuela Politécnica Superior, Universidad Autónoma de Madrid, 28049 Madrid, Spain (e-mail: hui.jiang01@estudiante.uam.es)

Juan Córcoles and Jorge A. Ruiz-Cruz are with the Applied Electromagnetics Group, Information Processing and Telecommunications Center, E.T.S. Ingenieros de Telecomunicación, Universidad Politécnica de Madrid, 28040 Madrid, Spain (email: juan.corcoles@upm.es; jorge.ruizcruz@upm.es)

This article was presented at the IEEE MTT-S International Microwave Symposium (IMS 2025), San Francisco, CA, USA, USA 15–20, 2025.

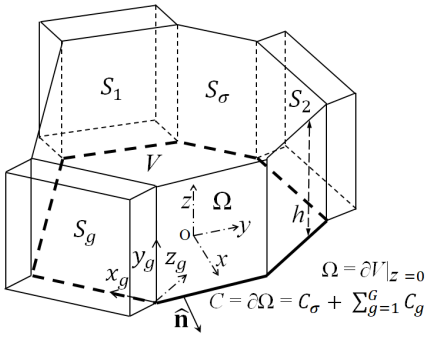

Fig. 1. *H*-plane junction with an arbitrary planar surface Ω and $g = 1, \ldots, G$ rectangular waveguide ports. The total contour is partitioned as $C = \partial\Omega = C_\sigma + \sum_g C_g$. The lids are the surfaces at $z = 0, h$, while the lateral walls corresponding to conductor are represented by S_σ.

This work aims to provide a computational efficient yet accurate approach to analyze *H*-plane waveguide devices including non-perfect conductor losses through a scalar 2D FEM. The proposed framework offers an alternative to 3D methods, making it particularly valuable for the early stages of design and optimization in waveguide-based microwave systems.

II. *H*-Plane Waveguide Modeling and Formulation

A. Ideal Lossless Formulation

We begin by formulating the 2D-FEM problem for *H*-plane waveguide devices, in the lossless case. The planar junction under consideration is illustrated in Fig. 1. The junction is divided into the homogeneous region V (the cavity) and the waveguide ports $g = 1, \ldots, G$. The volume V is laterally enclosed by a conductive surface S_σ, except at the reference planes S_g of the waveguide ports. The total lateral surface is denoted as $S_V = S_\sigma + \sum_{g=1}^{G} S_g$ with its normal vector pointing outward from the junction.

The fields in the cavity region V are obtained through the $\vec{\mathbf{A}}$ vector potential, and can be expressed as [11]

$$\vec{\mathbf{E}}^{(V)} = \frac{-k_p}{k_{tp}^2}\nabla_t e_z \sin(k_p z) + e_z \cos(k_p z)\hat{\mathbf{z}} \tag{1}$$

$$\vec{\mathbf{H}}^{(V)} = \frac{\mathrm{j}k}{k_{tp}^2\eta}\left(\nabla_t e_z \times \hat{\mathbf{z}}\right)\cos(k_p z) \tag{2}$$

where $k_p{=}\frac{p\pi}{h}$, p is a nonnegative integer, $k_{tp}^2 = k^2 - k_p^2$, $k = 2\pi f\sqrt{\mu\epsilon}$, $\eta = \sqrt{\mu/\epsilon}$, f is the frequency, and ϵ, μ are the electric permittivity and magnetic permeability, respectively, of the volume V. The scalar function $e_z(x, y)$ represents the longitudinal electric field in the cavity, excluding the dependence on the z coordinate. The transversal field at the ports can be expressed with a modal series [3], [5]:

$$\vec{\mathbf{E}}_t^{(g)}\Big|_{S_g} = \sum_{n=1}^{N_g}(a_n^{(g)} + b_n^{(g)})\vec{\mathbf{e}}_n^{(g)} \tag{3}$$

$$\vec{\mathbf{H}}_t^{(g)}\Big|_{S_g} = \sum_{n=1}^{N_g}(a_n^{(g)} - b_n^{(g)})\vec{\mathbf{h}}_n^{(g)} \tag{4}$$

The coefficients $a_n^{(g)}$ and $b_n^{(g)}$ represent the amplitudes of the incident and reflected modes and are used to compute the scattering parameters. For the problem in Fig. 1, *H*-plane excitation means that there is no field variation with respect to the z-axis of the cavity, which is the coordinate y_g associated to the height of the rectangular waveguide ports. Under fundamental mode excitation, the magnetic field has no component along y_g, and the modal basis at the ports is selected to be $\mathrm{TE}_{\mathfrak{m}0}^{z_g}$ [3], [5], with $p = 0$ in (1), (2). However, expressions in this work are written for the general case, required, for instance, when the device is connected to other components.

Numerical solution to the Helmholtz equation for the longitudinal field in (1),(2)

$$\nabla_t^2 e_z + k_{tp}^2 e_z = 0, \quad in\,\Omega, \tag{5}$$

with the boundary conditions for (1)-(4)

$$\hat{\mathbf{n}} \times \vec{\mathbf{E}}^{(V)} = \begin{cases} 0, & \text{in } S_\sigma, \\ \hat{\mathbf{n}} \times \vec{\mathbf{E}}^{(g)}, & \text{in } S_g,\ g = 1, \ldots, G \end{cases} \tag{6}$$

$$\hat{\mathbf{n}} \times \vec{\mathbf{H}}^{(V)} = \hat{\mathbf{n}} \times \vec{\mathbf{H}}^{(g)}, \quad \text{in } S_g,\ g = 1, \ldots, G \tag{7}$$

is addressed by a 2D FEM approach [5], interpolating e_z using scalar Lagrange basis functions $\alpha_m(x, y)$ with c_m being the M degrees of freedom (DoF) as:

$$e_z(x, y) = \sum_{m=1}^{M} c_m \alpha_m(x, y). \tag{8}$$

In this formulation, scalar basis function $\alpha_m(x, y)$ are employed due to the scalar nature of the proposed formulation, based on approximating a single scalar e_z field component, which provides a simpler implementation compared to vector basis functions. After discretization of the weak-form equations for this lossless problem, the following linear system is obtained:

$$\begin{cases} (\mathbf{S} - k_{tp}^2\mathbf{T})\mathbf{c} = \mathbf{E}(\mathbf{a} - \mathbf{b}), & M \text{ equations} \\ \mathbf{F}^t\mathbf{c} = \mathbf{Q}(\mathbf{a} + \mathbf{b}), & \sum_{g=1}^{G} N_g \text{ equations} \end{cases} \tag{9}$$

TABLE I
MATRIX DIMENSIONS

Matrices	$\mathbf{S}, \mathbf{T}, \mathbf{R}$	$\mathbf{E}, \mathbf{F}$	$\mathbf{Q}$
Dimension	$M \times M$	$M \times \sum_{g=1}^{G} N_g$	$\sum_{g=1}^{G} N_g \times \sum_{g=1}^{G} N_g$

where matrix elements in (9) are expressed as follows:

$$[\mathbf{S}]_{ji} = \iint_\Omega \nabla_t\alpha_j \cdot \nabla_t\alpha_i \, dS \tag{10}$$

$$[\mathbf{T}]_{ji} = \iint_\Omega \alpha_j\alpha_i \, dS \tag{11}$$

$$[\mathbf{E}]_{jn}^{(g)} = \left(\frac{k_{tp}^2\eta}{\mathrm{j}k}\right)\int_{C_g} \alpha_j \left(\vec{\mathbf{h}}_n^{(g)} \cdot \hat{\mathbf{x}}_g\right) dl \tag{12}$$

$$[\mathbf{Q}]_{nn}^{(g)} = \iint_{S_g} \left(\vec{\mathbf{e}}_n^{(g)} \times \vec{\mathbf{h}}_n^{(g)}\right) \cdot \hat{\mathbf{z}}_g \, dS \tag{13}$$

$$\mathbf{F}^{(g)} = \left(\zeta_{p0}\frac{h}{2}\right)\left(-\frac{\mathrm{j}k}{k_{tp}^2\eta}\right)\mathbf{E}^{(g)} \tag{14}$$

with $\zeta_{p0} = 1$ for $p > 0$,and $\zeta_{p0} = 2$ for $p = 0$. Matrices $\mathbf{E}$ and $\mathbf{F}$ are stacked by ports. Block diagonal matrix $\mathbf{Q}$ becomes the identity matrix when modes at all the ports are orthonormalized as usual. Table I summarizes the dimensions of the involved matrices.

From (9), the corresponding Generalized Impedance Matrix $\boldsymbol{\mathcal{Z}}$ and Generalized Scattering Matrix $\boldsymbol{\mathcal{S}}$ characterizing the device can be derived as:

$$(\mathbf{a} + \mathbf{b}) = \boldsymbol{\mathcal{Z}}(\mathbf{a} - \mathbf{b}), \quad \mathbf{b} = \boldsymbol{\mathcal{S}}\mathbf{a}, \tag{15}$$

$$\boldsymbol{\mathcal{Z}} = \mathbf{Q}^{-1}\mathbf{F}^t(\mathbf{S} - k_{tp}^2\mathbf{T})^{-1}\mathbf{E}, \tag{16}$$

$$\boldsymbol{\mathcal{S}} = (\boldsymbol{\mathcal{Z}} - \mathbf{I})(\boldsymbol{\mathcal{Z}} + \mathbf{I})^{-1} = \mathbf{I} - 2(\boldsymbol{\mathcal{Z}} + \mathbf{I})^{-1}, \tag{17}$$

where superscript t denotes the transpose operation.

B. Modeling Conductor Losses on Lid Surfaces

Modeling conductor losses on the lid surfaces (top and bottom walls perpendicular to z in Fig. 1) cannot be achieved numerically through a standard scalar 2D FEM formulation, since the only quantity being interpolated is e_z. In this case, an analytical approach is followed, in a similar way as proposed in [12].

Building upon the formulation for the ideal lossless case, we now extend the analysis to account for conductor losses on the lid surfaces. This is achieved by applying the Leontovich boundary condition [4], [11]

$$\vec{\mathbf{E}} - (\hat{\mathbf{n}}_s \cdot \vec{\mathbf{E}})\hat{\mathbf{n}}_s = -Z_s(\hat{\mathbf{n}}_s \times \vec{\mathbf{H}}) \tag{18}$$

at the lid surfaces to the cavity fields defined in (1), (2), where $\hat{\mathbf{n}}_s$ is the normal entering the conductor ($\mp\hat{\mathbf{z}}$ at the lids $z = 0, h$), Z_s is the surface impedance, usually expressed in terms of the skin depth $\delta = 1/\sqrt{\pi f\mu\sigma}$ for a material with electrical conductivity σ. By substituting (1), (2), into (18), we derive the following expression:

$$k_p \tan\left(k_p(z' + \frac{h}{2})\right) = \pm\mathrm{j}\frac{Z_s k}{\eta}, \tag{19}$$

where for convenience the longitudinal coordinate has been redefined as $z' = z - h/2$, and the fact that $\hat{\mathbf{n}} = \pm\hat{\mathbf{z}}$ at the lids $z' = \pm h/2$ has been used. For even p, it is fulfilled that $\tan(k_p(z' + \frac{h}{2})) = \tan(k_p z')$. Thus, the boundary conditions at the lids $z' = \pm h/2$ become a single expression

$$k_p \tan(k_p \frac{h}{2}) = \mathrm{j}\frac{Z_s k}{\eta}. \tag{20}$$

For $p = 0$ in usual H-plane excitation, (20) can be only fulfilled for $k_p = 0$ when $Z_s = 0$. However, we can find an approximate solution $\hat{k}_p \approx 0$ to (20) for small but non-zero Z_s. We rewrite (20) multiplying both sides by $\frac{h}{2}$

$$(\hat{k}_p \frac{h}{2}) \tan(\hat{k}_p \frac{h}{2}) = \mathrm{j}\frac{Z_s k h}{2\eta}, \tag{21}$$

and using $u \tan u \approx u^2$ for $u = \hat{k}_p h/2 \approx 0$, we get

$$(\hat{k}_p \frac{h}{2})^2 \approx \hat{k}_p \frac{h}{2} \tan(\hat{k}_p \frac{h}{2}) = \mathrm{j}\frac{Z_s k h}{2\eta}. \tag{22}$$

Since $\frac{Z_s}{k\eta} = (1 + \mathrm{j})\frac{\delta}{2}$, it is finally obtained

$$\hat{k}_p^2 = -(1 - \mathrm{j})\frac{\delta}{h} k^2, \tag{23}$$

and

$$k_{tp}^2 = k^2 - \hat{k}_p^2 = k^2 \left(1 + (1 - \mathrm{j})\frac{\delta}{h}\right). \tag{24}$$

C. Modeling Conductor Losses on Lateral Walls

To analyze conductor losses on lateral walls, the Leontovich boundary condition (18) is applied once again to the cavity fields given in (1) and (2), but this time at the lateral walls ($\hat{\mathbf{n}}_s = \hat{\mathbf{n}}$ in Fig. 1). This results in the following relationship:

$$\nabla_t e_z \cdot \hat{\mathbf{n}} = \mathrm{j}\frac{k_{tp}^2 \eta}{k Z_s} e_z. \tag{25}$$

Using (25) in the weak-form FEM discretization, the final system to characterize the H-plane device remains similar to (16), but with the inclusion of a new matrix component to account for conductor losses in lateral walls as follows:

$$\boldsymbol{\mathcal{Z}} = \mathbf{Q}^{-1}\mathbf{F}^t(\mathbf{S} - k_{tp}^2\mathbf{T} + \mathrm{j}\frac{k_{tp}^2\eta}{kZ_s}\mathbf{R})^{-1}\mathbf{E}, \tag{26}$$

where the elements of matrix $\mathbf{R}$ (dimension also listed in Table I) are defined as:

$$[\mathbf{R}]_{ji} = \int_{C_\sigma} \alpha_j \alpha_i dl. \tag{27}$$

Please note the integration in (27) is solely performed on the contour lines defining the lateral walls with nonperfect conductor, leaving out the ports.

III. Numerical Results

We validate the proposed model on four cases with increasing complexity: a rectangular waveguide section, a sinusoidal taper [13], an inductive filter with rounded corners [14] and a K-band diplexer. For lid losses, we use (16) with k_{tp}^2 from (24); for lateral wall losses, (26) with $k_{tp}^2 = k^2$; and for all losses, (26) with (24). The rectangular waveguide case

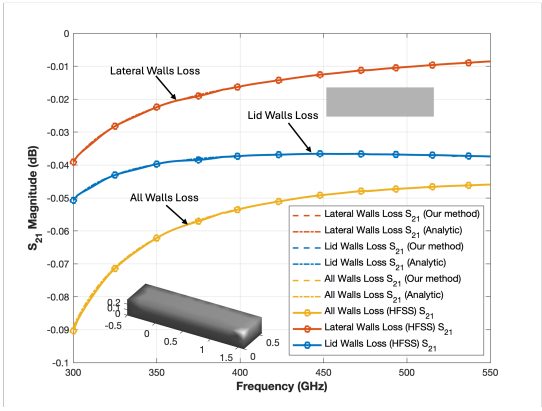

Fig. 2. Comparison of $|S_{21}|$ for a simple rectangular waveguide section with dimensions $a = 0.57\,\mathrm{mm}$, $b = 0.285\,\mathrm{mm}$, and length $d = 2.1\,\mathrm{mm}$. The waveguide conductivity is $\sigma = 5.8 \times 10^7\,\mathrm{S/m}$. Our method, analytic, and HFSS (with markers) responses are almost superimposed.

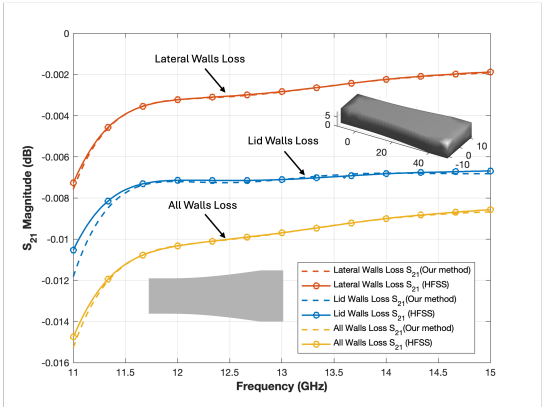

Fig. 3. Comparison of $|S_{21}|$ for a sinusoidal taper in WR90 waveguide [13] with conductivity of $\sigma = 5.8 \times 10^7\,\mathrm{S/m}$. Our method and HFSS (with markers) responses are almost superimposed.

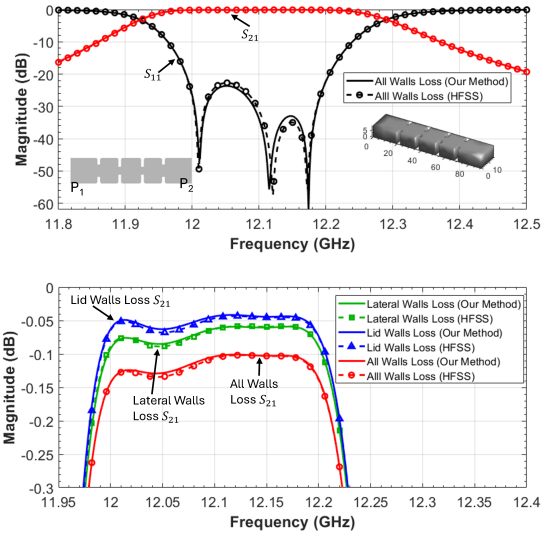

Fig. 4. Comparison of $|S_{11}|$ and $|S_{21}|$ for a third-order H-plane filter in WR75 with rounded corners [14] with conductivity of $\sigma = 5.8 \times 10^7\,\mathrm{S/m}$. HFSS response (with markers) almost superimposed to our method.

TABLE II
COMPARISON OF DEGREES OF FREEDOM (DOF) BETWEEN HFSS AND OUR METHOD FOR CONVERGENT (ALMOST OVERLAPPING) RESULTS

	Fig. 2	Fig. 3	Fig. 4	Fig. 5
DoF (HFSS)	10696	10714	361938	5152415
DoF (Our Method)	3009	4804	27295	132110

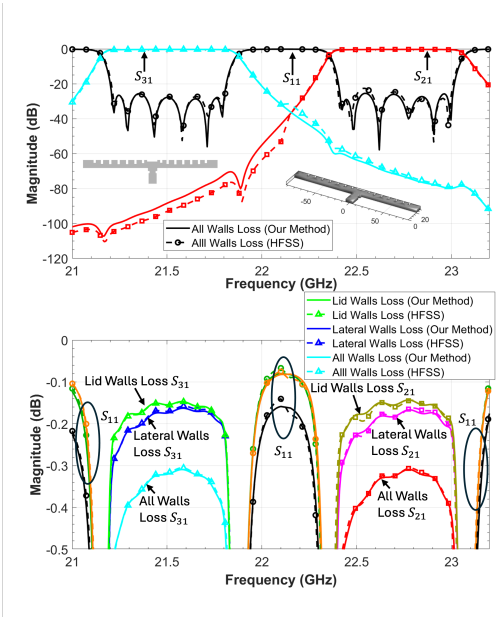

Fig. 5. Comparison of the full-wave response for a K-band diplexer with inductive filters having asymmetric irises, with conductivity of $\sigma = 5.8 \times 10^7\,\mathrm{S/m}$. The HFSS response (with markers) is almost superimposed on the proposed method.

serves as a baseline, showing excellent agreement with both an analytical solution (via the power loss method [15]) and HFSS results (see Fig. 2). The taper and filter cases (Fig. 3 and 4) further demonstrate the model's accuracy in more complex geometries, while the diplexer in Fig. 5 confirms its robustness.

A key advantage of our approach is its 2D formulation, which significantly reduces the number of DoF relative to 3D-FEM solvers. This reduction translates into lower memory usage and faster simulations, especially as the geometry becomes more intricate. Another benefit is the straightforward way losses can be included separately on the lid or lateral walls, making it easy to identify which surfaces predominantly contribute to the total dissipation. As shown in Table II, the number of DoF required by our method for a nearly overlapping result is consistently much lower than that of HFSS, illustrating both its computational efficiency and flexibility.

IV. CONCLUSION

A novel 2D-FEM framework for *H*-plane waveguide analysis has been validated against analytical and HFSS results. Its 2D formulation greatly enhances computational efficiency, facilitating iterative design. Moreover, independently computing lid and lateral wall losses provides valuable insights into device performance. Overall, this model is a robust alternative to 3D full-wave solvers for waveguide design and optimization.

REFERENCES

[1] J. Uher, J. Bornemann, and U. Rosenberg, *Waveguide components for antenna feed systems: Theory and CAD*. Artech House, 1993.

[2] R. J. Cameron, C. M. Kudsia, and R. R. Mansour, *Microwave filters for communication systems: fundamentals, design, and applications*. John Wiley & Sons, 2018.

[3] M. Guglielmi, R. Sorrentino, and G. Conciauro, *Advanced Modal Analysis: CAD Techniques for Waveguide Components and Filter*. John Wiley & Sons, Inc., 1999.

[4] J. Jin, *The Finite Element Method in Electromagnetics*, 3rd ed. Wiley-IEEE Press, 2014.

[5] G. Pelosi, R. Coccioli, and S. Selleri, *Quick Finite Elements for Electromagnetic Waves*, ser. Artech House electromagnetic analysis series. Artech House, 2009.

[6] J. Webb and S. Porihar, "Finite element analysis of H-plane rectangular waveguide problem," *Proceedings IEE*, vol. 133, no. 2, pp. 91–94, 1986.

[7] M. Koshiba and M. Suzuki, "Finite-element analysis of H-plane waveguide junction with arbitrarily shaped ferrite post," *IEEE Transactions on Microwave Theory and Techniques*, vol. 34, no. 1, pp. 103–109, 1986.

[8] K. Ise and M. Koshiba, "Numerical analysis of H-plane waveguide junctions by combination of finite and boundary elements," *IEEE Transactions on Microwave Theory and Techniques*, vol. 36, no. 9, pp. 1343–1351, 1988.

[9] G. G. Gentili, L. Accatino, and G. Bertin, "The generalized 2.5-D finite-element method for analysis of waveguide components," *IEEE Transactions on Microwave Theory and Techniques*, vol. 64, no. 8, pp. 2392–2400, 2016.

[10] L. Codecasa, C. D'Asta, G. G. Gentili, M. Bozzi, and L. Perregrini, "Advanced modeling of SIW structures by 2-D finite element method," *IEEE Transactions on Microwave Theory and Techniques*, vol. 71, no. 7, pp. 2818–2827, 2023.

[11] C. Balanis, *Advanced Engineering Electromagnetics*. Wiley, 2012.

[12] A. Melloni and G. Gentili, "Modellization of losses in TE/sub 011/-mode waveguide bandpass filters," *IEEE Transactions on Microwave Theory and Techniques*, vol. 43, no. 11, pp. 2642–2644, 1995.

[13] G. Garcia-Contreras, J. Córcoles, J. A. Ruiz-Cruz, M. Oldoni, G. G. Gentili, S. Micheletti, and S. Perotto, "Advanced modeling of rectangular waveguide devices with smooth profiles by hierarchical model reduction," *IEEE Transactions on Microwave Theory and Techniques*, vol. 71, no. 11, pp. 4692–4702, 2023.

[14] G. Conciauro, P. Arcioni, M. Bressan, and L. Perregrini, "Wideband modeling of arbitrarily shaped H-plane waveguide components by the "boundary integral-resonant mode expansion method"," *IEEE Transactions on Microwave Theory and Techniques*, vol. 44, no. 7, pp. 1057–1066, 1996.

[15] R. E. Collin, *Field theory of guided waves*. John Wiley & Sons, 1990, vol. 5.